

# Superconductivity near an Ising nematic quantum critical point in two dimensions

Jie Huang,<sup>1</sup> Zhao-Kun Yang,<sup>1</sup> Jing-Rong Wang,<sup>2</sup> and Guo-Zhu Liu<sup>1,\*</sup>

<sup>1</sup>*Department of Modern Physics, University of Science and Technology of China, Hefei, Anhui 230026, China*

<sup>2</sup>*High Magnetic Field Laboratory of Anhui Province,  
Chinese Academy of Sciences, Hefei 230031, China*

Near a two-dimensional Ising-type nematic quantum critical point, the quantum fluctuations of the nematic order parameter are coupled to the electrons, leading to non-Fermi liquid behavior and unconventional superconductivity. The interplay between these two effects has been extensively studied through the Eliashberg equations for the superconducting gap. However, previous studies often rely on various approximations that may introduce uncertainties in the results. Here, we revisit this problem without these approximations and examine how their removal changes the outcomes. We numerically solve four self-consistent Eliashberg integral equations of the mass renormalization  $A_1(p)$ , the chemical potential renormalization  $A_2(p)$ , the pairing function  $\Phi(p)$ , and the nematic self-energy (polarization) function  $\Pi(q)$  using the iteration method. Our calculations retain the explicit non-linearity and the full momentum dependence of these equations. We find that discarding some commonly used approximations allows for a more accurate determination of the superconducting gap  $\Delta = \Phi/A_1$  and the critical temperature  $T_c$ . The Eliashberg equations have two different convergent gap solutions: an extended  $s$ -wave gap and a  $d_{x^2-y^2}$ -wave gap. The latter is fragile, whereas the former is robust against small perturbations.

## I. INTRODUCTION

Electronic nematic order refers to a state of matter that spontaneously breaks the  $C_4$ -symmetry down to  $C_2$ -symmetry. Investigations of this order date back to Kivelson, Fradkin, and Emery [1], who first proposed the existence of electronic nematicity in the normal state of high- $T_c$  cuprate superconductors as a result of stripe melting. The electronic nematicity can also be understood via an alternative scenario [2, 3]: the Pomeranchuk instability of the Fermi surface. For a system exhibiting such an order, the resistivity and other observable quantities are strongly anisotropic. Experimentally, clear signatures of the electronic nematic order has been observed in various condensed matter systems, including cuprates [4–14], iron-based superconductors [15–28], some heavy-fermion superconductor [29],  $\text{Sr}_2\text{RuO}_4$  [30], Kagome superconductors [31–33], magic-angle graphene [34, 35], and superconducting nickelate [36].  $\text{FeSe}$  [18, 19] and  $\text{Ba}_{1-x}\text{Sr}_x\text{Ni}_2\text{As}_2$  [37] are of particular interest because they display nematic order but do not exhibit magnetic order, highlighting the unique role of the nematic fluctuations. Many of these superconductors share two common properties: the presence of a dome-shaped transition line for the superconducting state and the emergence of non-Fermi liquid (NFL) behavior in the normal state.

The electronic nematic phase transition occurs at zero temperature when a non-thermal parameter  $x$ , such as carrier density or pressure, is tuned to a critical value  $x_c$ , defining a nematic quantum critical point (QCP). For  $x > x_c$ , the system is tetragonal, while for  $x < x_c$  it is orthogonal. Although the nematic order parameter has a vanishing expectation value at the QCP  $x = x_c$ , i.e.,

$\langle \phi \rangle = 0$ , nematic quantum fluctuations are significant and strongly interact with the gapless electrons near the Fermi surface. This interaction is usually described by a Yukawa-type fermion-boson coupling. The physical effects of this coupling have been studied for decades by employing various analytical and numerical techniques [2, 3, 38–58]. A general consensus is that this coupling can induce NFL behavior at high temperatures and unconventional superconductivity at low temperatures under appropriate conditions. These effects are most significant at the QCP and diminish as the system is tuned away from the QCP. Quantum criticality vanishes entirely once the system becomes sufficiently far from the QCP. These general features offer a promising explanation for the aforementioned two common features of unconventional superconductors.

In this paper, we revisit the quantum criticality of an Ising-type nematic transition in two spatial dimensions and study the properties of the superconductivity that emerges from the NFL state near the nematic QCP. The nematic order is assumed to have  $d$ -wave symmetry, characterized by an anisotropic form factor in the Yukawa coupling term. For simplicity, we only consider the disordered side of nematic transition, where  $x \geq x_c$ . In the limits of  $x \gg x_c$  and  $x \rightarrow x_c$ , the system behaves as a normal FL and a typical NFL, respectively. Within the broad intermediate range of  $x$ , the system resides in a mixed FL/NFL regime, exhibiting FL behavior at low energies and NFL behavior at high energies.

The NFL behavior and superconductivity are both induced by the same Yukawa coupling, implying that they mutually influence each other. As a result, they must be treated on an equal footing. In a number of previous works [42, 47, 54, 57, 58], their interplay has been addressed based on the Eliashberg theory [59]. From a technical perspective, the self-consistent Eliashberg integral equations for the renormalization factors and Cooper

\*Corresponding author: gzliu@ustc.edu.cn

pairing function are highly nonlinear and challenging to solve. To reduce numerical difficulty, a series of approximations have been introduced in practical computations [42, 47, 54, 57, 58].

The boson polarization function  $\Pi(q)$ , i.e., the boson self-energy, determines the effective strength of the Yukawa coupling and thus plays a crucial role in the theoretical description of the superconducting transition. In previous studies,  $\Pi(q)$  is generically computed up to the leading one-loop level within the framework of perturbation expansion [42, 47, 54, 57, 58], along with certain additional approximations. This polarization is oversimplified as it disregards the impact of the NFL behavior and Cooper pairing on the dynamical properties of the nematic fluctuations.

Another commonly used approximation is to consider only the electrons located exactly on the Fermi surface [42, 47, 54, 57, 58], achieved by fixing the absolute value of the electron momentum  $\mathbf{p}$  at the Fermi momentum  $\mathbf{p}_F$ . Under this approximation, the difficulty of numerical computations is greatly reduced. However, this approximation is invalid for superconductivity developed in the NFL regime, where the electrons occupy a considerable portion of states off the Fermi surface. To determine the gap size and  $T_c$  with higher precision, it is essential to take into account the contributions from the full range of electron momenta.

In the close vicinity of the critical temperature  $T_c$ , the pairing gap  $\Phi \rightarrow 0$ . Taking advantage of this feature, one can employ a linearization approximation. Although this approximation has been frequently used [42, 47, 54] due to its ability to greatly simplify numerical computations, it may introduce large uncertainties in the gap size at temperatures well below  $T_c$ . In addition, the linearized equations are not capable of capturing the mutual influence between Cooper pairing and other many-body correlation effects (i.e., Landau damping, mass renormalization).

In this work, we focus on weak Yukawa couplings and investigate the formation of superconductivity mediated by nematic fluctuations using the Eliashberg theory, assuming that the vertex corrections are negligible. Apart from the bare vertex assumption, we avoid employing any additional approximations. We will directly solve the self-consistently coupled non-linear integral equations of the wave-function renormalization  $A_1(p)$ , the mass renormalization factor  $A_2(p)$ , the Cooper pairing function  $\Delta(p)$ , and the polarization  $\Pi(q)$  without adopting the linearization and Fermi surface approximations. Based on the numerical solutions, we are able to examine determine the pairing gap at any temperature below  $T_c$  with a relatively higher accuracy.

Our findings show that the nematic fluctuations lead to different gap symmetries: an extended  $s$ -wave symmetry and a  $d_{x^2-y^2}$ -wave symmetry. The former symmetry is robust against small perturbations, whereas the latter is fragile and exist only under special conditions. Superconducting  $T_c$  is found to be maximal at the nematic

QCP and is rapidly suppressed as the system moves away from the QCP. Accordingly, the superconducting boundary displays a dome-shaped curve on the  $T$ - $x$  plane. We also solved the simplified equations by making a number of widely used approximations and compared the results with those obtained without these approximations. We find that the introduction of various approximations do not change the order parameter symmetry, but lead to quantitatively inaccurate results of the gap size and the superconducting  $T_c$ .

The rest of the paper is arranged as follows. In Sec. II, we define the effective model of the nematic quantum critical system and present the Eliashberg integral equations. In Sec. III, we present the numerical results of these equations and analyze their physical implications. A brief summary of the results is given in Sec. IV.

## II. EFFECTIVE MODEL OF THE SYSTEM

We consider a  $(2+1)$ -dimensional field theory that describes the interaction between the gapless electrons and the nematic quantum fluctuations, which is expressed as

$$\mathcal{L} = \psi^\dagger (i\epsilon_n - \xi_{\mathbf{p}}) \psi - g_0 \hat{f}(\mathbf{p}) \phi \psi^\dagger \psi + \phi^\dagger ((i\omega_m)^2 - \mathbf{q}^2 - r) \phi, \quad (1)$$

where  $\psi$  and  $\phi$  are the field operators of electrons and nematic fluctuations, respectively. Within the Matsubara formalism, the electron frequencies are  $\epsilon_n = (2n+1)\pi T$  and the boson frequencies are  $\omega_m = 2m\pi T$ . The electron dispersion is  $\xi_{\mathbf{p}} = \frac{\mathbf{p}^2}{2m} - E_F$ , where  $E_F$  is the Fermi energy. The boson mass  $r$  serves as the non-thermal that tunes the nematic quantum phase transition at  $T = 0$ , with  $r = 0$  defines the nematic QCP. Our current interest is restricted to the disordered side of nematic phase transition, which is described by a positive  $r$ . The self-coupling  $(\phi^\dagger \phi)^2$  is usually an irrelevant perturbation, especially near the QCP, and thus is not included. The effective strength of the Yukawa coupling is strongly anisotropic, characterized by a constant  $g$  and an angle-dependent form factor  $\hat{f}(\mathbf{p})$ . Following Lederer *et al.* [42] and Klein *et al.* [56], we consider a  $d$ -wave form factor:

$$\hat{f}(\mathbf{p}) = \frac{p_x^2 - p_y^2}{p_x^2 + p_y^2}. \quad (2)$$

Use the standard Nambu spinor  $\Psi$  [60] and Pauli matrices, we re-write the Lagrangian density as follows

$$\mathcal{L} = \Psi^\dagger (i\epsilon_n \sigma_0 - \xi_{\mathbf{p}} \sigma_3) \Psi - g_0 \hat{f}(\mathbf{p}) \phi \Psi^\dagger \sigma_0 \Psi + \phi^\dagger ((i\omega_m)^2 - \mathbf{q}^2 - r) \phi. \quad (3)$$

The free electron propagator is

$$G_0(p) \equiv G_0(\epsilon_n, \mathbf{p}) = \frac{1}{i\epsilon_n \sigma_0 - \xi_{\mathbf{p}} \sigma_3}, \quad (4)$$

and the free boson propagator is

$$D_0(q) \equiv D_0(\omega_m, \mathbf{q}) = \frac{1}{(i\omega_m)^2 - \mathbf{q}^2 - r}. \quad (5)$$

The free and renormalized electron propagators satisfy the following Dyson-Schwinger (DS) equation

$$G^{-1}(p) = G_0^{-1}(p) - ig \int_q \hat{f}^2(\mathbf{q}, \mathbf{p}) \sigma_3 G(p+q) \times D(q) \Gamma_v(q, p), \quad (6)$$

where  $G(p)$  is the full electron propagator,  $D(q)$  is the full boson propagator, and  $\Gamma_v(q, p)$  is the vertex function. The abbreviations  $\int_q \equiv \int \frac{dq}{(2\pi)^3}$  and  $g = g_0^2$  are used. The DS equation of the boson propagator  $D(q)$  has the form

$$D^{-1}(q) = D_0^{-1}(q) - \Pi(q), \quad (7)$$

where the polarization function is

$$\Pi(q) = g \text{Tr} \int_p \hat{f}^2(\mathbf{q}, \mathbf{p}) \sigma_3 G(p) \Gamma_v(q, p) G(p+q). \quad (8)$$

The DS equations of  $G(p)$  and  $D(q)$  cannot be solved without detailed knowledge of the vertex function  $\Gamma_v(q, p)$ . Unfortunately, there is currently no satisfactory method to determine  $\Gamma_v(q, p)$ . Here, we assume that the coupling parameter  $g$  takes small values and the tuning parameter  $r$  is not very small. Under these conditions, the vertex corrections can be approximately neglected.

We thus make the replacement  $\Gamma_v(q, p) \rightarrow \sigma_3$  and obtain the following Eliashberg equations:

$$G^{-1}(p) = G_0^{-1}(p) - ig \int_q \hat{f}^2(\mathbf{q}, \mathbf{p}) \sigma_3 G(p+q) \sigma_3 D(q), \quad (9)$$

$$D^{-1}(q) = D_0^{-1}(q) - g \text{Tr} \int_p \hat{f}^2(\mathbf{q}, \mathbf{p}) \sigma_3 G(p) \sigma_3 G(p+q) \quad (10)$$

The renormalized electron propagator  $G(p)$  can be generically written in the form

$$G(p) = \frac{1}{A_1(\epsilon_n, \mathbf{p}) \epsilon_n \sigma_0 - A_2(\epsilon_n, \mathbf{p}) \xi_{\mathbf{p}} \sigma_3 + \Phi(\epsilon_n, \mathbf{p}) \sigma_1} \quad (11)$$

As demonstrated by Nambu [60], the  $\sigma_2$  term needs not be considered.  $A_1(\epsilon_n, \mathbf{p})$ ,  $A_2(\epsilon_n, \mathbf{p})$ , and  $\Phi(\epsilon_n, \mathbf{p})$  are known as the mass renormalization, the chemical potential renormalization, and the Cooper pairing function. By solving the self-consistent equations of these three functions, the interaction-induced quantum many-body effects and their mutual influence can be simultaneously determined. The superconducting gap is defined as

$$\Delta(\epsilon_n, \mathbf{p}) = \frac{\Phi(\epsilon_n, \mathbf{p})}{A_1(\epsilon_n, \mathbf{p})}. \quad (12)$$

Substituting Eq. (11) into Eq. (9), we decompose the equations of  $G(p)$  into three self-consistent integral equations of  $A_1(\epsilon_n, \mathbf{p})$ ,  $A_2(\epsilon_n, \mathbf{p})$ , and  $\Phi(\epsilon_n, \mathbf{p})$  given by

$$A_1(\epsilon_n, \mathbf{p}) = 1 + \frac{T}{\epsilon_n} \sum_m \int \frac{d^2 \mathbf{q}}{(2\pi)^2} \tilde{\mathcal{K}}_v(\omega_m, \epsilon_n; \mathbf{q}, \mathbf{p}) A_1(\epsilon_n + \omega_m, \mathbf{p} + \mathbf{q})(\epsilon_n + \omega_m), \quad (13)$$

$$A_2(\epsilon_n, \mathbf{p}) = 1 - \frac{T}{\xi_{\mathbf{p}}} \sum_m \int \frac{d^2 \mathbf{q}}{(2\pi)^2} \tilde{\mathcal{K}}_v(\omega_m, \epsilon_n; \mathbf{q}, \mathbf{p}) A_2(\epsilon_n + \omega_m, \mathbf{p} + \mathbf{q}) \xi_{\mathbf{p}+\mathbf{q}}, \quad (14)$$

$$\Phi(\epsilon_n, \mathbf{p}) = T \sum_m \int \frac{d^2 \mathbf{q}}{(2\pi)^2} \tilde{\mathcal{K}}_v(\omega_m, \epsilon_n; \mathbf{q}, \mathbf{p}) \Phi(\epsilon_n + \omega_m, \mathbf{p} + \mathbf{q}), \quad (15)$$

where the kernel function  $\tilde{\mathcal{K}}_v$  has the form

$$\tilde{\mathcal{K}}_v(\omega_m, \epsilon_n; \mathbf{q}, \mathbf{p}) = \frac{g \hat{f}^2(\mathbf{q}, \mathbf{p})}{\omega_m^2 + |\mathbf{q}|^2 + r + \Pi(\omega_m, \mathbf{q})} \times \frac{1}{A_1^2(\epsilon_n + \omega_m, \mathbf{p} + \mathbf{q})(\epsilon_n + \omega_m)^2 + A_2^2(\epsilon_n + \omega_m, \mathbf{p} + \mathbf{q}) \xi_{\mathbf{p}+\mathbf{q}}^2 + \Phi^2(\epsilon_n + \omega_m, \mathbf{p} + \mathbf{q})}. \quad (16)$$

Substituting Eq. (11) into Eq. (8) leads to the following equation satisfied by the polarization:

$$\Pi(\omega_m, \mathbf{q}) = gT \sum_n \int \frac{d^2 \mathbf{p}}{(2\pi)^2} \frac{\hat{f}^2(\mathbf{q}, \mathbf{p})}{[A_1^2(\epsilon_n, \mathbf{p}) \epsilon_n^2 + A_2^2(\epsilon_n, \mathbf{p}) \xi_{\mathbf{p}}^2 + \Phi^2(\epsilon_n, \mathbf{p})]} \times \frac{A_1(\epsilon_n + \omega_m, \mathbf{p} + \mathbf{q}) A_1(\epsilon_n, \mathbf{p}) - A_2(\epsilon_n + \omega_m, \mathbf{p} + \mathbf{q}) \xi_{\mathbf{p}+\mathbf{q}} A_2(\epsilon_n, \mathbf{p}) \xi_{\mathbf{p}} + \Phi(\epsilon_n + \omega_m, \mathbf{p} + \mathbf{q}) \Phi(\epsilon_n, \mathbf{p})}{[A_1^2(\epsilon_n + \omega_m, \mathbf{p} + \mathbf{q})(\epsilon_n + \omega_m)^2 + A_2^2(\epsilon_n + \omega_m, \mathbf{p} + \mathbf{q}) \xi_{\mathbf{p}+\mathbf{q}}^2 + \Phi^2(\epsilon_n + \omega_m, \mathbf{p} + \mathbf{q})]}. \quad (17)$$

For the convenience of numerical calculations, we re-scale all the variables appearing in the integral equations with respect to either the Fermi energy  $E_F$  or the Fermi momentum  $p_F$  as follows:

$$\begin{aligned}\epsilon_n &\rightarrow \frac{\epsilon_n}{E_F}, & \omega_m &\rightarrow \frac{\omega_m}{E_F}, & T &\rightarrow \frac{T}{E_F}, \\ \mathbf{q} &\rightarrow \frac{\mathbf{q}}{p_F}, & \mathbf{p} &\rightarrow \frac{\mathbf{p}}{p_F}, & \xi_{\mathbf{p}} &\rightarrow \frac{\xi_{\mathbf{p}}}{E_F} = \mathbf{p}^2 - 1, \\ A_1 &\rightarrow A_1, & A_2 &\rightarrow A_2, & \Phi &\rightarrow \frac{\Phi}{E_F}, \\ g &\rightarrow \frac{g}{E_F}, & r &\rightarrow \frac{r}{p_F^2}.\end{aligned}$$

After such re-scaling transformations, all the variables become dimensionless.

The above set of coupled integral equations is highly complicated and hard to solve via numerical techniques. To make numerical computations simpler, a variety of approximations have been extensively adopted in previous works [42, 54, 55, 57, 58], as discussed in Sec. I. For instance, the polarization function  $\Pi(q)$  is generically calculated up to the one-loop level at zero temperature. The zero- $T$  one-loop polarization, defined via the free electron propagator as

$$\Pi^{1L}(q) = g \text{Tr} \int_p \hat{f}(\mathbf{q}, \mathbf{p}) \sigma_3 G_0(p) \sigma_3 G_0(p+q), \quad (18)$$

has the following analytical form

$$\Pi^{1L}(q) \approx -\frac{g}{4\pi} \tilde{f}^2 \frac{|\omega_m|}{|\mathbf{q}|} \quad (19)$$

in the limit  $|\omega_m| \ll |\mathbf{q}|$ . Inserting this polarization into Eq. (7) leads to

$$D^{1L}(q) = \frac{1}{(i\omega_m)^2 - \mathbf{q}^2 - r + \Pi^{1L}(q)}. \quad (20)$$

The boson kinetic term  $\omega^2$  is often neglected due to its relatively small magnitude compared to  $\Pi^{1L}(q)$  at low energies. However, we choose to retain this term.

Apart from the one-loop polarization approximation, there are several other widely employed approximations, including fixing the electron momentum  $\mathbf{p}$  at the Fermi momentum  $p_F$ , called Fermi surface approximation, and the neglect of the chemical potential renormalization realized by setting  $A_2(p) = 1$ . When implementing the Fermi surface approximation, rather than strictly fixing  $\mathbf{p}$  at  $p_F$ , we assume that all the electrons within a thin shell of thickness  $\lambda E_F$ , where  $\lambda$  is a small dimensionless parameter, around the Fermi surface participate in the formation of superconductivity. Through a series of detailed derivations, the original set of four integral equations is simplified to

$$A_1(\epsilon_n, \theta_{\mathbf{p}}) = 1 + \frac{T}{\epsilon_n} \sum_m \int \frac{d\theta_{\mathbf{p}+\mathbf{q}}}{(2\pi)} \tilde{\mathcal{K}}_b(\omega_m, \epsilon_n; \theta_{\mathbf{p}+\mathbf{q}}, \theta_{\mathbf{p}}) A_1(\epsilon_n + \omega_m, \theta_{\mathbf{p}+\mathbf{q}}), \quad (21)$$

$$\Phi(\epsilon_n, \theta_{\mathbf{p}}) = T \sum_m \int \frac{d\theta_{\mathbf{p}+\mathbf{q}}}{(2\pi)} \tilde{\mathcal{K}}_b(\omega_m, \epsilon_n; \theta_{\mathbf{p}+\mathbf{q}}, \theta_{\mathbf{p}}) \Phi(\epsilon_n + \omega_m, \theta_{\mathbf{p}+\mathbf{q}}), \quad (22)$$

where we have defined the following three functions

$$\begin{aligned}\tilde{\mathcal{K}}_b(\omega_m, \epsilon_n; \theta_{\mathbf{p}+\mathbf{q}}, \theta_{\mathbf{p}}) &= \frac{g_f \tilde{f}^2(\theta_{\mathbf{p}+\mathbf{q}}, \theta_{\mathbf{p}})}{\omega_m^2 + 2(1 - \cos(\theta_{\mathbf{p}+\mathbf{q}} - \theta_{\mathbf{p}})) + r - \Pi^{1L}(\omega_m, \theta_{\mathbf{p}+\mathbf{q}}, \theta_{\mathbf{p}})} \\ &\quad \times \frac{1}{A_1^2(\epsilon_n + \omega_m, \theta_{\mathbf{p}+\mathbf{q}})(\epsilon_n + \omega_m)^2 + \Phi^2(\epsilon_n + \omega_m, \theta_{\mathbf{p}+\mathbf{q}})},\end{aligned} \quad (23)$$

$$\Pi^{1L}(\omega_m, \theta_{\mathbf{p}+\mathbf{q}}, \theta_{\mathbf{p}}) = -\frac{g_f \tilde{f}^2(\theta_{\mathbf{p}+\mathbf{q}}, \theta_{\mathbf{p}}) |\omega_m|}{8\pi \left| \sin\left(\frac{1}{2}(\theta_{\mathbf{p}+\mathbf{q}} - \theta_{\mathbf{p}})\right) \right|}, \quad (24)$$

$$\tilde{f}(\theta_{\mathbf{p}+\mathbf{q}}, \theta_{\mathbf{p}}) = \frac{1}{4} [\cos(2\theta_{\mathbf{p}+\mathbf{q}}) + \cos(2\theta_{\mathbf{p}}) + 2\cos(\theta_{\mathbf{p}+\mathbf{q}} + \theta_{\mathbf{p}})]. \quad (25)$$

Here, a new coupling parameter  $g_f = g\lambda$  is introduced to implement the Fermi surface approximation. In the calculations, we choose  $\lambda = 0.1$ .

One could further linearize these equations by omitting the pairing function  $\Phi$  from the denominators near  $T_c$ . However, we choose not to do so, as our interest extends beyond the narrow temperature range around  $T_c$ .

### III. NUMERICAL RESULTS

The effective field theory of nematic quantum criticality considered here has been investigated by Lederer *et al.* [42] and Klein and Chubukov [54] by employing various approximations, including but not restricted to those outlined in Sec. II. Lederer *et al.* [42] focused on

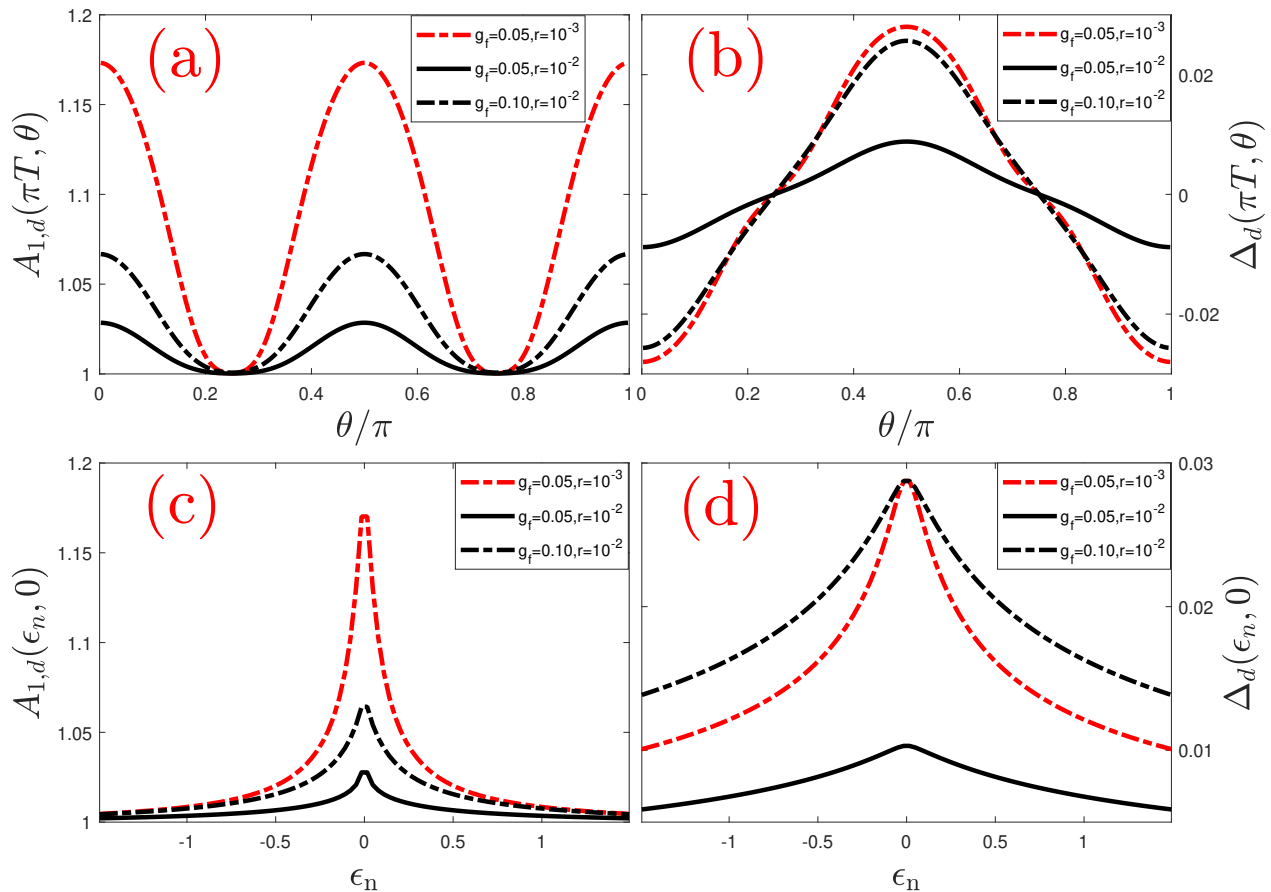


FIG. 1: Results for the  $d_{x^2-y^2}$ -wave gap obtained from solutions of simplified equations (21)-(22) at the temperature  $T = 0.01$ . (a)-(b) show the angle dependence of the renormalization factor  $A_{1,d}(\theta)$  and the  $d_{x^2-y^2}$ -wave superconducting gap  $\Delta_d(\theta)$  at the frequency  $\epsilon_n = \pi T$ . (c)-(d) show the frequency dependence of  $A_{1,d}(\epsilon_n)$  and  $\Delta_s(\epsilon_n)$  for a given angle  $\theta = 0$ . Solid and dashed lines of the same color have the same coupling constant  $g_f = 0.05$  ( $g = 0.5$  and  $\lambda = 0.1$ ), while the dashed lines of different colors correspond to the same  $r = 0.01$ .

the BCS-Eliashberg regime of the model, characterized by a relatively large value of boson mass  $r$ , and revealed an obvious enhancement of superconductivity upon approaching the nematic QCP in both  $s$ -wave and  $d$ -wave channels. In comparison, Klein and Chubukov [54] studied the true NFL regime at the nematic QCP with  $r = 0$ . In addition to the approximations discussed above, the renormalization factor  $A_1(p)$  adopted in Ref. [54] was computed perturbatively up to the one-loop level in the normal state where the gap vanishes. While their results incorporate the influence of the NFL behavior on the formation of Cooper pairs, they neglect the reverse influence of the Cooper pairing on NFL behavior. An anisotropic  $s$ -wave pairing gap was found in Ref. [54]. Recently, a highly anisotropic  $s$ -wave superconducting gap has been observed [61] near the nematic QCP of  $\text{FeSe}_{1-x}\text{S}_x$ , which is qualitatively consistent with the gap symmetry predicted in Ref. [54].

In this paper, we will focus on small values of  $r$ , which correspond to the NFL regime. But we do not consider

the exact nematic QCP with  $r = 0$ , because the Eliashberg theory may become less reliable in such a deep NFL regime. We deem it essential to develop efficient methods for accurately computing the superconducting gap and  $T_c$ . Our aim is to elucidate how the previously obtained results are altered when the commonly used approximations are removed. For this purpose, we directly solve the  $(2+1)$ -dimensional non-linear integral equations given by Eqs. (13)-(17) and then compare our new results with those obtained by solving the simplified equations given by Eqs. (21)-(22).

We first solve the simplified non-linear integral equations given by Eqs. (21)-(22) numerically by means of the iteration method demonstrated in Ref. [62]. The numerical solutions will be used to determine the symmetry of the superconducting order parameter and extract the dependence of the maximum superconducting gap and the critical temperature  $T_c$  on parameters  $r$  and  $g$ . It is also interesting to judge whether the boson zero frequency plays an important role.

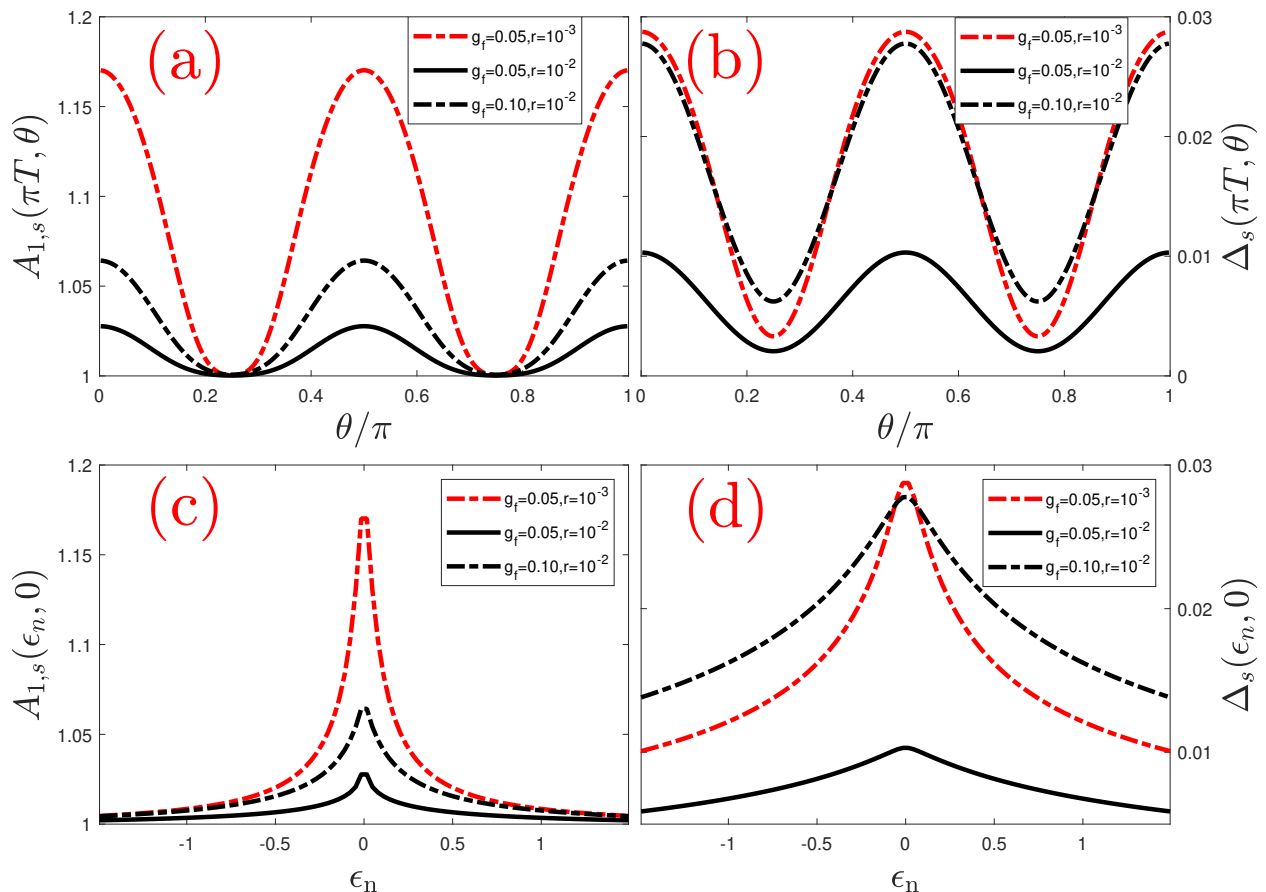


FIG. 2: Results for the  $s$ -wave gap obtained from solutions of simplified equations (21)-(22) at the temperature  $T = 0.01$ . (a)-(b) show the angle dependence of the renormalization factor  $A_{1,s}(\theta)$  and the  $s$ -wave superconducting gap  $\Delta_s(\theta)$  at the frequency  $\epsilon_n = \pi T$ . (c)-(d) show the frequency dependence of  $A_{1,s}(\epsilon_n)$  and  $\Delta_s(\epsilon_n)$  for a given angle  $\theta = 0$ . Solid and dashed lines of the same color have the same coupling constant  $g_f = 0.05$  ( $g = 0.5$  and  $\lambda = 0.1$ ), while the dashed lines of different colors correspond to the same  $r = 0.01$ .

### A. Superconducting order parameter symmetry

Although the form factor  $\hat{f}(\theta)$  of the Yukawa coupling exhibits a  $d$ -wave angular dependence, the resulting pairing gap does not necessarily display  $d$ -wave symmetry [42]. To determine the pairing symmetry, we numerically solve the nonlinear integral equations using various initial values of  $\Phi(p)$  and analyze the angular dependence of the convergent solutions for the gap  $\Delta(p)$ .

We find that, if a pure  $d_{x^2-y^2}$ -wave initial value of  $\Phi(p)$  is assumed, the numerical solutions have converged into a pure  $d_{x^2-y^2}$ -wave superconducting gap described by  $\Delta_d = \Delta_0[\cos(\pi \cos \theta) - \cos(\pi \sin \theta)]$ . The corresponding solutions for  $A_{1,d}$  and  $\Delta_d$  are presented in Fig. 1. From (a) and (b), one can see that both  $A_{1,d}(\theta)$  and  $\Delta_d(\theta)$  are strongly dependent of the angle  $\theta$ . The absolute values of these two quantities are maximal in the anti-nodal directions ( $0, \pi/2, \pi, 3\pi/2$ ) and minimal in the nodal directions ( $\pi/4, 3\pi/4, 5\pi/4, 7\pi/4$ ). Notably, the sign of  $\Delta_d(\theta)$  changes with the variation of  $\theta$ . The maxima of  $A_{1,d}$  and  $\Delta_d$  exhibit an obvious dependence on the parameters  $g$

and  $r$ . Specifically, for a fixed value of  $r$ , these maxima increase as  $g$  grows. Conversely, for a fixed value of  $g$ , they are suppressed as  $r$  increases. As shown by (c) and (d) of Fig. 1, both  $A_{1,d}(\epsilon_n, \theta = 0)$  and  $\Delta_d(\epsilon_n, \theta = 0)$  exhibit peaks at the smallest electron frequency, but they are rapidly suppressed at higher frequencies.

Alternatively, one could assign a  $\theta$ -independent constant initial value to  $\Phi(p)$ . After numerous iterations, a stable and convergent  $s$ -wave pairing solution has been obtained, regardless of the initial value. Such an  $s$ -wave pairing is identified as an extended  $s$ -wave gap, as the gap remains positive for all angles. This finding aligns with the results of Klein and Chubukov [54] and is also consistent with the observation reported in Nag *et al.* [61]. In Fig. 2, we present the detailed  $\theta$ -dependence of the corresponding  $A_{1,s}(\theta)$  and  $\Delta_s(\theta)$  at the frequency  $\epsilon_n = \pi T$ , as well as the detailed  $\epsilon_n$ -dependence of  $A_{1,s}(\epsilon_n)$  and  $\Delta_s(\epsilon_n)$  at the angle  $\theta = 0$ . Similar to the case of  $d_{x^2-y^2}$ -wave pairing, the  $s$ -wave superconductivity is enhanced for smaller values of  $r$  and larger values of  $g$ .

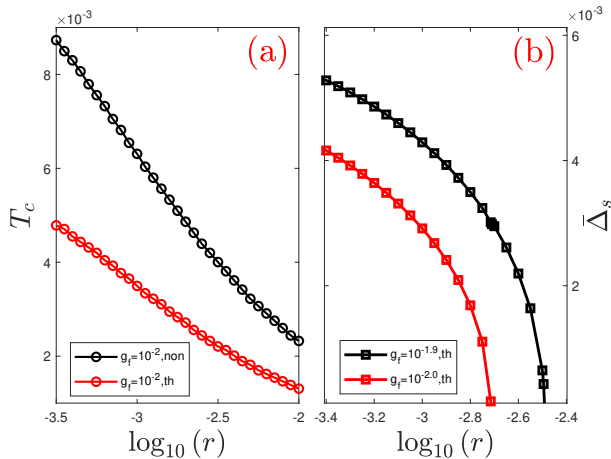


FIG. 3: (a) shows the  $r$ -dependence of  $T_c$  obtained at  $g = 0.01$  for  $s$ -wave gap. The red and black lines represent the results obtained in the presence and absence of thermal effects, respectively. (b) shows the  $r$ -dependence of averaged  $s$ -wave gap that includes thermal effects.

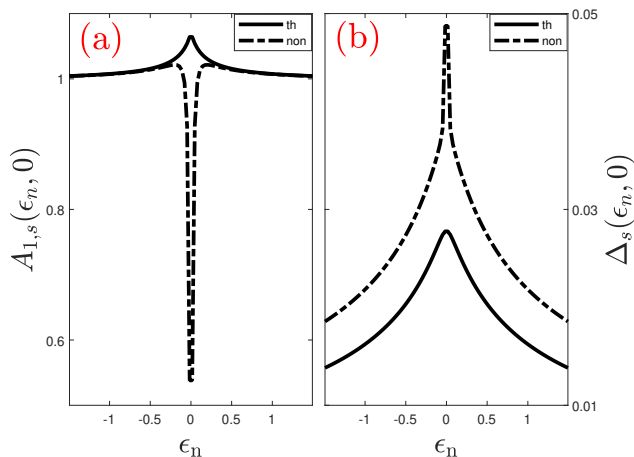


FIG. 4: The energy (frequency) dependence of  $A_1(i\epsilon_n)$  and  $\Delta_s(i\epsilon_n)$ . The solid and dashed lines stand for the results obtained with (th) and without (non) considering thermal effects.

It is necessary to analyze the stability of the  $d_{x^2-y^2}$ -wave and the extended  $s$ -wave pairings. To this end, we consider initial pairing functions ( $\Phi$ ) that display a variety of angular dependencies on  $\theta$ , extending beyond the pure  $d_{x^2-y^2}$ -wave form. Our results indicate that all assigned initial gaps ultimately converge to exactly the same extended  $s$ -wave gap. Notably, the integral equations do not support gap solutions that break the time-reversal symmetry, such as the  $d + is$ -wave pairing. It appears that nematic fluctuations favor either  $d_{x^2-y^2}$ -wave pairing or extended  $s$ -wave pairing, with no other possibilities. Of these two pairings, the  $d_{x^2-y^2}$ -wave pairing is not stable, as it only persists when the initial gap

is strictly in the  $d_{x^2-y^2}$ -wave form. The presence of even a very small additional component in the initial  $d_{x^2-y^2}$ -wave gap leads to the extended  $s$ -wave pairing emerging as the sole stable solution. Therefore, in the subsequent discussions, we consider only extended  $s$ -wave pairing.

## B. Dependence of the gap size and $T_c$ on $r$

Numerical results demonstrate that the gap size is a decreasing function of the boson mass  $r$ . According to Fig. 2, for a fixed  $g$ , the maxima of  $A_{1,s}(\theta)$  and  $\Delta_s(\theta)$  are obviously reduced if  $r$  becomes larger. This is consistent with the general understanding that nematic fluctuations become more pronounced as the system approaches the nematic QCP. Once  $r$  exceeds a certain critical value  $r_c$ , which depends on  $g$ , the nematic fluctuations are too weak to induce the Cooper pairing instability. The  $r$ -dependence of  $T_c$  and the averaged  $s$ -wave gap are illustrated in Fig. 3(a) and Fig. 3(b), respectively. It is clear that the superconductivity achieved near the nematic QCP is rapidly suppressed when  $r$  is increasing. These findings suggest the existence of a dome-shaped boundary for the superconducting phase, at least on the nematic-disordered side.

## C. Role of the thermal effects

In some theoretical studies [47, 54] on superconductivity mediated by nematic fluctuations, the thermal effects, which are represented by the contribution from the boson zero frequency (i.e.,  $\omega_m = 0$ ), are neglected. While neglecting the boson zero frequency may be justified under certain special conditions, it is not generally valid. To investigate the impact of thermal effects, we have solved the integral equations both with and without including these effects. Our calculations reveal that the results for the quantities  $A_1$  and  $\Delta_{s,d}$  are significantly different. Therefore, the thermal effects are explicitly considered in all the results shown in Fig. 1 and Fig. 2.

As can be seen from the curves illustrated in Fig. 3(a), ignoring the thermal effects leads to a considerable overestimation of the critical temperature  $T_c$ . In Fig. 4, we show the frequency dependence of  $A_{1,s}(\epsilon_n, \theta = 0)$  and  $\Delta_s(\epsilon_n, \theta = 0)$ . The neglect of thermal effects leads to an anomalously sharp suppression of  $A_{1,s}(\epsilon_n, \theta = 0)$  at low frequencies, which in turn results in a dramatic enhancement of  $\Delta_s(\epsilon_n, \theta = 0)$ . It turns out that such effects are unphysical and arise from the improper omission of the boson zero frequency.

## D. Beyond the widely used approximations

The results discussed in Figs.1-4 are obtained from the solutions of the simplified non-linear equations (21)-(22). We now examine to what extent these results are

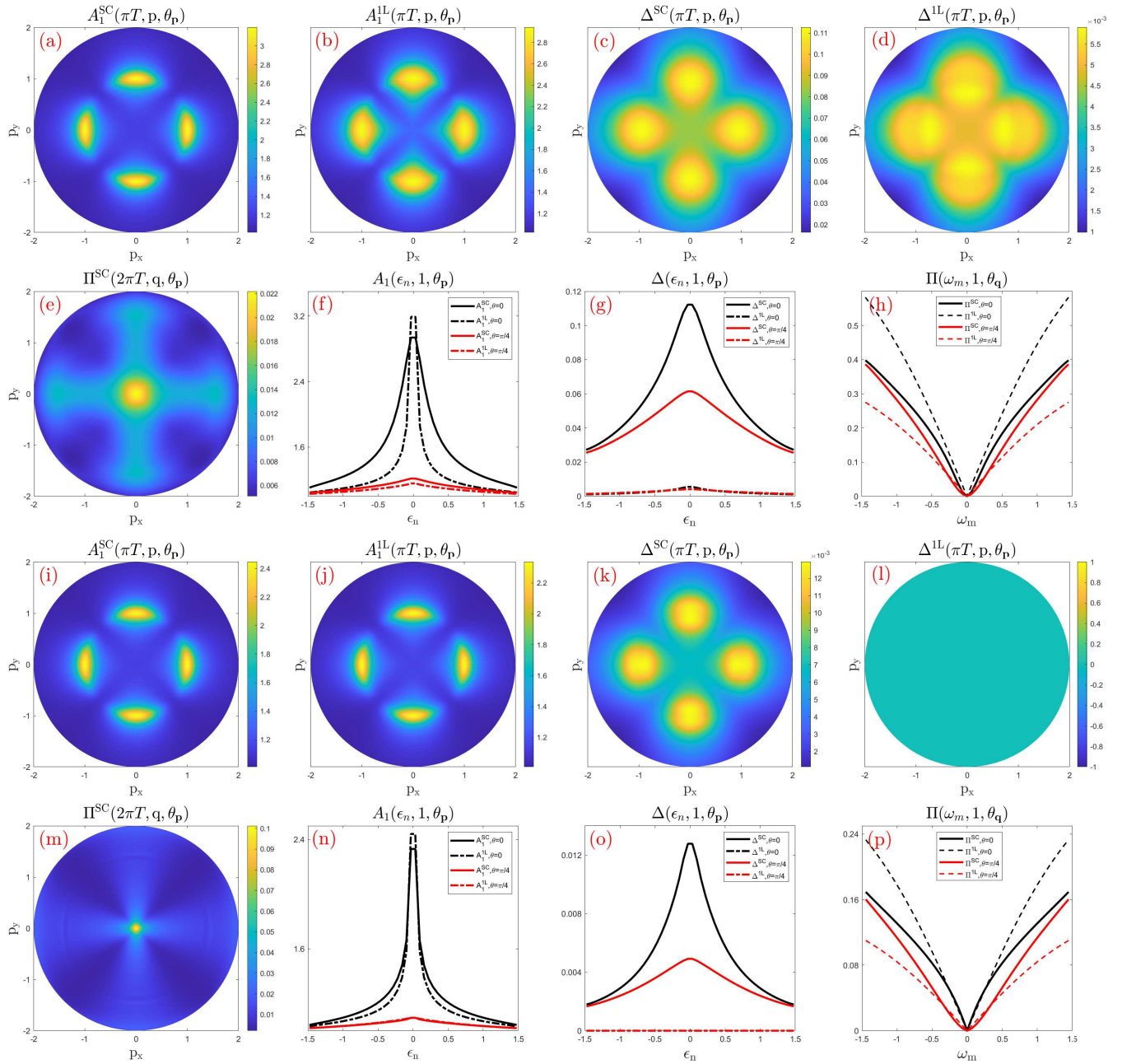


FIG. 5: Results obtained at  $r = 0.01$  and  $T = 0.01$ . The parameter  $g = 0.5$  for (a)-(h) and  $g = 0.2$  for (i)-(p).

changed if the approximations summarized in Sec. II are removed. We have solved the original integral equations (13)-(15) and present the results in Fig. 5. The thermal effects are explicitly included. From now on, we focus solely on the stable  $s$ -wave pairing and hence adopt the simplified notation  $\Delta$  to denote the extended  $s$ -wave superconducting gap.

It is more efficient to numerically solve non-linear integral equations at higher temperatures. To reduce the computational load, we consider relatively large values of  $g$ , so as to ensure larger values of  $T_c$ . We first set  $g = 0.5$ ,  $r = 0.01$ , and  $T = 0.01$ , and then obtain

the full frequency-momentum dependence of  $A_1(\epsilon_n, \mathbf{p})$ ,  $A_2(\epsilon_n, \mathbf{p})$ ,  $\Delta(\epsilon_n, \mathbf{p})$ , and  $\Pi(\omega_m, \mathbf{q})$ . Due to limited space, we do not show the results of  $A_2(\epsilon_n, \mathbf{p})$  and present the solutions of the rest three functions in Fig. 5 (a)-(h).

Among the sub-figures of Fig. 5, (a) and (b) show the color maps of the renormalization functions  $A_1^{\text{SC}}$  and  $A_1^{\text{1L}}$  obtained using the self-consistent polarization, denoted by  $\Pi^{\text{SC}}(q)$ , and one-loop polarization, denoted by  $\Pi^{\text{1L}}(q)$ , respectively. (c) and (d) show the color maps of the superconducting gap  $\Delta^{\text{SC}}$  and  $\Delta^{\text{1L}}$  obtained by using  $\Pi^{\text{SC}}(q)$  and  $\Pi^{\text{1L}}(q)$ , respectively. (e) shows the color map of the self-consistent polarization  $\Pi(q)$  on the momentum



plane. In sub-figures (a)-(e), the frequency is fixed. The frequency-dependence of the relevant functions are depicted in (f)-(g), where the electron momentum is fixed at  $p_F$  and the angle  $\theta = 0, \pi/4$ . There is an obvious quantitative distinction between the results of  $A_1(\epsilon_n, \mathbf{p}_F)$  and  $\Delta(\epsilon_n, \mathbf{p}_F)$  determined based on  $\Pi^{\text{SC}}(q)$  and those determined based on  $\Pi^{\text{1L}}(q)$ . This difference arises from the obvious deviation of  $\Pi^{\text{1L}}(q)$  from  $\Pi^{\text{SC}}(q)$ . One can see from (h) that  $\Pi^{\text{1L}}(q)$  is a good approximation of  $\Pi^{\text{SC}}(q)$  only within a very small range of  $\omega_m$ .

Owing to the significantly increased computational time in the limit  $T \rightarrow T_c$ , we have not determined the value of  $T_c$  with a sufficiently high accuracy. To estimate the impact of different forms of the polarization on  $T_c$ , we consider a smaller  $g$  with  $g = 0.2$ , meanwhile retaining  $r = 0.01$  and  $T = 0.01E_F$ , and present the corresponding results in (i)-(p) of Fig. 5. (i) and (j) show the color maps of  $A_1^{\text{SC}}$  and  $A_1^{\text{1L}}$ , respectively. (k) and (l) show the color maps of  $\Delta^{\text{SC}}$  and  $\Delta^{\text{1L}}$ , respectively. (m) shows the color map of  $\Pi^{\text{SC}}(q)$  on the momentum plane. (n)-(p) are the counterparts of (f)-(h). The superconducting gap  $\Delta$  is nonzero if  $\Pi^{\text{SC}}(q)$  is used, but vanishes if  $\Pi^{\text{1L}}(q)$  is used. This is a clear indication that  $\Pi^{\text{1L}}(q)$  yields a considerably lower  $T_c$  compared to  $\Pi^{\text{SC}}(q)$ . A simple comparison between (n) and (o) indicates that the strong suppression of superconductivity due to one-loop  $\Pi^{\text{1L}}(q)$  arises from two joint effects:  $\Pi^{\text{1L}}(q)$  at  $\theta = 0$  is substantially larger than  $\Pi^{\text{SC}}(q)$  at  $\theta = 0$  within a wide frequency range; the use of  $\Pi^{\text{1L}}(q)$  amplifies the maximum of  $A_1(\theta = 0)$ . Another notable distinction between  $\Pi^{\text{1L}}(q)$  and  $\Pi^{\text{SC}}(q)$  lies in their dependence on the angle  $\theta$ :  $\Pi^{\text{1L}}(q)$  is strongly dependent of  $\theta$ , whereas  $\Pi^{\text{SC}}(q)$  changes only moderately with the variation in  $\theta$ .

Now, let us compare the black solid line in Fig. 2(d) with the black dashed line in Fig. 5(g). The former is obtained using  $\Pi^{\text{1L}}(q)$  combined with the Fermi surface approximation, with parameters  $\theta = 0$ ,  $r = 0.01$ ,  $T = 0.01$ ,  $g = 0.5$ ,  $\lambda = 0.1$ . The latter is obtained using  $\Pi^{\text{1L}}(q)$  with  $\theta = 0$ ,  $r = 0.01$ ,  $T = 0.01$ , and  $g = 0.5$ , but without employing the Fermi surface approximation. It is evident that removing the Fermi surface approximation slightly leads to a slight reduction of the gap size.

#### IV. SUMMARY

In summary, we have investigated the interplay between the NFL behavior and superconductivity using an effective field theory that describes the physics of a two-dimensional metal near an Ising-type nematic QCP. Within this framework, the Yukawa coupling between electrons and nematic fluctuations is characterized by a strongly anisotropic  $d$ -wave form factor. After numerically solving the non-linear Eliashberg equations obeyed by the renormalization functions  $A_1(\epsilon_n, \mathbf{p})$  and  $A_2(\epsilon_n, \mathbf{p})$ , the pairing function  $\Delta(\epsilon_n, \mathbf{p})$ , and the polarization function  $\Pi(\epsilon_n, \mathbf{p})$ , we have verified that the extended  $s$ -wave superconducting gap is the only stable and convergent

solution. The maximum value of the  $s$ -wave gap and the critical temperature  $T_c$  are larger values when the system is close to the QCP, but are strongly suppressed as the system moves away from the QCP. Our results indicate that commonly used one-loop polarization  $\Pi^{\text{1L}}(\epsilon_n, \mathbf{p})$  significantly deviates from the self-consistently calculated polarization. Consequently, it is not recommended to use  $\Pi^{\text{1L}}(\epsilon_n, \mathbf{p})$  for an accurate determination of the gap size and  $T_c$  accurately. Additionally, the use of Fermi surface approximation also leads to quantitatively inaccurate results.

Understanding the microscopic pairing mechanisms of unconventional superconductors is of paramount scientific importance. Typically, several potential mechanisms could induce superconductivity. To identify the true origin of superconductivity, it is necessary to accurately calculate the superconducting gap and the value of  $T_c$  for each mechanism and compare the results to determine which mechanism is most plausible. Previous calculations have relied on various approximations, some of which tend to overestimate  $T_c$ , while others underestimate it. When multiple approximations are employed simultaneously, determining the true value of  $T_c$  becomes particularly challenging. It is therefore imperative to perform calculations with as few approximations as possible.

The primary distinction between our work and previous studies is that our calculations extend beyond several widely used approximations. We assume that the nematic model is within the adiabatic regime, thereby validating the Eliashberg theory, or equivalently, rendering the vertex corrections negligible. For the results presented in Sec. III D, no additional approximations beyond this assumption are employed.

The reliability of our results hinges on the validity of Eliashberg theory. While our calculations have surpassed several typical approximations to achieve greater accuracy, they still rely on the bare vertex approximation. As the system is tuned very close to the nematic QCP, the vertex corrections become increasingly significant and can no longer be ignored, especially in the limit  $r \rightarrow 0$ . To fully address the interplay between NFL behavior and superconductivity at the nematic QCP, it is important to go beyond Eliashberg theory and incorporate the contributions of the vertex corrections. We would like to explore the impact of vertex corrections on our current results in future work.

#### V. ACKNOWLEDGEMENT

We thank the helpful discussion with Hao-Fu Zhu. This work is supported by the Anhui Natural Science Foundation under Grant 2208085MA11. J.R.W. acknowledges the support by the National Natural Science Foundation of China under Grant 12274414. The numerical calculations in this paper have been done on the supercomputing system in the Supercomputing Center of University of Science and Technology of China.

- 
- [1] S. A. Kivelson, E. Fradkin, and V. Emery, Electronic liquid-crystal phases of a doped Mott insulator, *Nature (London)* **393**, 550 (1998).
- [2] V. Oganesyan, S. A. Kivelson, and E. Fradkin, Quantum theory of a nematic Fermi fluid, *Phys. Rev. B* **64**, 195109 (2001).
- [3] W. Metzner, D. Rohe, and S. Andergassen, Soft Fermi Surfaces and Breakdown of Fermi-Liquid Behavior, *Phys. Rev. Lett.* **91**, 066402 (2003).
- [4] Y. Ando, K. Segawa, S. Komiya, and A. N. Lavrov, Electrical resistivity anisotropy from self-Organized one dimensionality in high-temperature superconductors, *Phys. Rev. Lett.* **88**, 137005 (2002).
- [5] E. Fradkin, S. A. Kivelson, and J. M. Tranquada, Colloquium: Theory of intertwined orders in high temperature superconductors, *Rev. Mod. Phys.* **87**, 457 (2015).
- [6] B. Keimer, S. A. Kivelson, M. R. Norman, S. Uchida, and J. Zaanen, From quantum matter to high-temperature superconductivity in copper oxides, *Nature* **518**, 179 (2015).
- [7] V. Hinkov, D. Haug, B. Fauqué, P. Bourges, Y. Sidis, A. Ivanov, C. Bernhard, C. T. Lin, B. Kerimer, Electronic liquid crystal state in the high-temperature superconductor  $\text{YBa}_2\text{Cu}_3\text{O}_{6.45}$ , *Science* **319**, 597 (2008).
- [8] R. Daou, J. Chang, D. LeBoeuf, O. Cyr-Choinière, F. Laliberté, N. Doiron-Leyraud, B. J. Ramshaw, R. Liang, D. A. Bonn, W. N. Hardy, and L. Taillefer, Broken rotational symmetry in the pseudogap phase of a high- $T_c$  superconductor, *Nature* **463**, 519 (2010).
- [9] M. J. Lawler, K. Fujita, J. Lee, A. R. Schmidt, Y. Kohsaka, C. K. Kim, H. Eisaki, S. Uchida, J. C. Davis, J. P. Sethna, and E. A. Kim, Intra-unit-cell electronic nematicity of the high- $T_c$  copper-oxide pseudogap states, *Nature* **466**, 347 (2010).
- [10] Y. Sato, S. Kasahara, H. Murayama, Y. Kasahara, E.-G. Moon, T. Nishizaki, T. Loew, J. Porras, B. Keimer, T. Shibauchi, and T. Matsuda, Thermodynamic evidence for a nematic phase transition at the onset of the pseudogap in  $\text{YBa}_2\text{Cu}_3\text{O}_y$ , *Nat. Phys.* **13**, 1074 (2017).
- [11] J. Wu, A. T. Bollinger, X. He, and Božović, Spontaneous breaking of rotational symmetry in copper oxide superconductors, *Nature* **547**, 432 (2017).
- [12] N. Auvray, S. Benhabib, M. Cazayous, R. D. Zhong, J. Schneeloch, G. D. Gu, A. Forget, D. Colson, I. Paull, A. Sacuto, and Y. Gallais, Nematic fluctuations in the cuprate superconductor  $\text{Bi}_2\text{Sr}_2\text{CaCu}_2\text{O}_{8+\delta}$ , *Nat. Commun.* **10**, 5209 (2019).
- [13] S. Mukhopadhyay, R. Sharma, C. K. Kim, S. D. Edkins, M. H. Hamidian, H. Eisaki, Shin-ichi Uchida, E.-A. Kim, M. J. Lawler, A. P. Mackenzie, J. C. Séamus Davis, and K. Fujita, Evidence for a vestigial nematic state in the cuprate pseudogap phase, *Proc. Natl. Acad. Sci.* **116**, 13249 (2019).
- [14] K. Ishida, S. Hosoi, Y. Teramoto, T. Usui, Y. Mizukami, K. Itaka, Y. Matsuda, T. Watanabe, and T. Shibauchi, Divergent nematic susceptibility near the pseudogap critical point in a cuprate superconductor, *J. Phys. Soc. Jpn.* **89**, 064707 (2020).
- [15] A. Chubukov, Pairing Mechanism in Fe-Based Superconductors, *Ann. Rev. Condens. Matter Phys.* **3**, 57 (2012).
- [16] R. M. Fernandes, A. V. Chubukov, and J. Schmalian, Nematic order in iron superconductors: who is in the driver seat?, *Nat. Phys.* **10**, 97 (2014).
- [17] T. Shibauchi, A. Carrington, and Y. Matsuda, A quantum critical point lying beneath the superconducting dome in iron pnictides, *Ann. Rev. Condens. Matter Phys.* **5**, 113 (2014).
- [18] A. Coldea and M. D. Watson, The key ingredients of the electronic structure of FeSe, *Ann. Rev. Condens. Matter Phys.* **9**, 125 (2018).
- [19] A. E. Böhrer and A. Kreisel, Nematicity, magnetism and superconductivity in FeSe, *J. Phys. Condens. Matter* **30**, 023001 (2017).
- [20] T.-M. Chuang, M. P. Allan, J. Lee, Y. Xie, N. Ni, S. L. Bud'ko, G. S. Boebinger, P. C. Canfield, J. C. Davis, Nematic Electronic Structure in the Parent State of the Iron-Based Superconductor  $\text{Ca}(\text{Fe}_{1-x}\text{Co}_x)_2\text{As}_2$ , *Science* **327**, 181 (2010).
- [21] J.-H. Chu, J. G. Analytis, K. De Greve, P. L. McMahon, Z. Islam, Y. Yamamoto, and I. R. Fisher, In-plane resistivity anisotropy in an underdoped ironArsenide superconductor, *Science* **329**, 824 (2010).
- [22] C.-L. Song, Y.-L. Wang, P. Cheng, Y.-P. Jiang, W. Li, T. Zhang, Z. Li, K. He, L. Wang, J.-F. Jia, H.-H. Hung, C. Wu, X. Ma, X. Chen, and Q.-K. Xue, Direct observation of nodes and twofold symmetry in FeSe superconductor, *Science* **332**, 1410 (2011).
- [23] S. Kasahara, H. J. Shi, K. Hashimoto, S. Tonegawa, Y. Mizukami, T. Shibauchi, K. Sugimoto, T. Fukuda, T. Terashima, A. H. Nevidomskyy, and Y. Matsuda, Electronic nematicity above the structural and superconducting transition in  $\text{BaFe}_2(\text{As}_{1-x}\text{P}_x)_2$ , *Nature* **486**, 328 (2012).
- [24] X. Lu, J. T. Park, R. Zhang, H. Luo, A. H. Nevidomsky, Q. Si, and P. Dai, Nematic spin correlations in the tetragonal state of uniaxial-strained  $\text{BaFe}_{2-x}\text{Ni}_x\text{As}_2$ , *Science* **345**, 657 (2014).
- [25] S.-H. Baek, D. V. Efremov, J. M. Ok, J. S. Kim, J. van den Brink, and B. Büchner, Orbital-driven nematicity in FeSe, *Nat. Mat.* **14**, 210 (2015).
- [26] H.-H. Kuo, J.-H. Chu, J. C. Palmstrom, S. A. Kivelson, and I. R. Fisher, Ubiquitous signatures of nematic quantum criticality in optimally doped Fe-based superconductors, *Science* **352**, 358 (2016).
- [27] C. A. Occhialini, J. J. Sanchez, Q. Song, G. Fabbris, Y. Choi, J.-W. Kim, P. J. Ryan, and R. Comin, Spontaneous orbital polarization in the nematic phase of FeSe, *Nat. Mat.* **22**, 985 (2023).
- [28] K. Mukasa, K. Ishida, S. Imajo, M. Qiu, M. Saito, K. Matsuura, Y. Sugimura, S. Liu, Y. Uezono, T. Otsuka, M. Čulo, S. Kasahara, Y. Matsuda, N. E. Hussey, T. Watanabe, K. Kindo, and T. Shibauchi, Enhanced superconducting pairing strength near a pure nematic quantum critical point, *Phys. Rev. X* **13**, 011032 (2023).
- [29] F. Ronning, T. Helm, K. R. Shirer, M. D. Bachmann, L. Balicas, M. K. Chan, B. J. Ramshaw, R. D. McDonald, F. F. Balakirev, M. Jaime, E. D. Bauer, and P. J. W. Moll, Electronic in-plane symmetry breaking at field-tuned quantum criticality in  $\text{CeRhIn}_5$ , *Nature* **548**, 313 (2017).
- [30] J. Wu, H. P. Nair, A. T. Bollinger, X. He, I. Robinson, N. J. Schreiber, K. M. Shen, D. G. Schlom, and I. Božović,

- Electronic nematicity in  $\text{Sr}_2\text{RuO}_4$ , *Proc. Natl. Acad. Sci.*, **117**, 10654 (2020).
- [31] L. Nie, S. Sun, W. Ma, D. Song, L. Zhang, Z. Liang, P. Wu, F. Yu, J. Li, M. Shan, D. Zhao, S. Li, B. Kang, Z. Wu, Y. Zhou, K. Liu, Z. Xiang, Z. Yang, Z. Wang, T. Wu, and X. Chen, Charge-density-wave-driven electronic nematicity in a kagome superconductor, *Nature* **604**, 59 (2022).
- [32] P. Wu, Y. Tu, Z. Wang, S. Yu, H. Li, W. Ma, Z. Liang, Y. Zhang, X. Zhang, Z. Li, Y. Yang, Z. Qiao, J. Ying, T. Wu, L. Shan, Z. Xiang, Z. Wang, and X. Chen, Unidirectional electron-phonon coupling in the nematic state of a kagome superconductor, *Nat. Phys.* **19**, 1143 (2023).
- [33] Y. Hu, C. Le, Y. Zhang, Z. Zhao, J. Liu, J. Ma, N. C. Plumb, M. Radovic, H. Chen, A. P. Schnyder, X. Wu, X. Dong, J. Hu, H. Yang, H.-J. Gao, M. Shi, Non-trivial band topology and orbital-selective electronic nematicity in a titanium-based kagome superconductor, *Nat. Phys.* **19**, 1827 (2023).
- [34] Y. Cao, D. Rodan-Legrain, J. M. Park, N. F. Q. Yuan, K. Watanabe, T. Taniguchi, R. M. Fernandes, L. Fu, P. Jarillo-Herrero, Nematicity and competing orders in superconducting magic-angle graphene, *Science* **327**, 264 (2021).
- [35] Y. Jiang, X. Lai, K. Watanabe, T. Taniguchi, K. Haule, J. Mao, and E. Y. Andrei, Charge-order and broken rotational symmetry in magic angle twisted bilayer graphene, *Nature* **573**, 91 (2019).
- [36] H. Ji, Y. Liu, Y. Li, X. Ding, Z. Xie, C. Ji, S. Qi, X. Gao, M. Xu, P. Gao, L. Qiao, Y.-F. Yang, G.-M. Zhang, and J. Wang, Rotational symmetry breaking in superconducting nickelate  $\text{Nd}_{0.8}\text{Sr}_{0.2}\text{NiO}_2$  films, *Nat. Commun.* **14**, 7155 (2017).
- [37] C. Eckberg, D. J. Campbell, T. Metz, J. Collini, H. Hodovanets, T. Drye, P. Zavalij, M. H. Christensen, R. M. Fernandes, S. Lee, P. Abbamonte, J. W. Lynn, and J. Paglione, Sixfold enhancement of superconductivity in a tunable electronic nematic system, *Nat. Phys.* **16**, 346 (2020).
- [38] L. Dell'Anna and W. Metzner, Fermi surface fluctuations and single electron excitations near Pomeranchuk instability in two dimensions, *Phys. Rev. B* **73**, 045127 (2006).
- [39] J. Rech, C. Pépin, A. V. Chubukov, Quantum critical behavior in itinerant electron systems: Eliashberg theory and instability of a ferromagnetic quantum critical point, *Phys. Rev. B* **74**, 195126 (2006).
- [40] M. A. Metlitski and S. Sachdev, Quantum phase transitions of metals in two spatial dimensions. I. Ising-nematic order, *Phys. Rev. B* **82**, 075127 (2010).
- [41] H. Yamase and R. Zeyher, Superconductivity from orbital nematic fluctuations, *Phys. Rev. B* **88**, 180502(R) (2013).
- [42] S. Lederer, Y. Schattner, E. Berg, S. Kivelson, Enhancement of superconductivity near a nematic quantum critical point, *Phys. Rev. Lett.* **114**, 097001 (2015).
- [43] M. A. Metlitski, D. F. Mross, S. Sachdev, and T. Senthil, Cooper pairing in non-Fermi liquids, *Phys. Rev. B* **91**, 115111 (2015).
- [44] T. Maier and D. J. Scalapino, Pair structure and the pairing interaction in a bilayer Hubbard model for unconventional superconductivity, *Phys. Rev. B* **90**, 174510 (2014).
- [45] M. Eimenkel, H. Meier, C. Pépin, and K. B. Efetov, Pairing gaps near ferromagnetic quantum critical points, *Phys. Rev. B* **91**, 064507 (2015).
- [46] S. Raghu, G. Torroba, and H. Wang, Metallic quantum critical points with finite BCS couplings, *Phys. Rev. B* **92**, 205104 (2015).
- [47] Y. Wang, A. Abanov, B. L. Altshuler, E. A. Yuzbashyan, and A. V. Chubukov, Superconductivity near a quantum-critical point: The special role of the first Matsubara frequency, *Phys. Rev. Lett.* **117**, 157001 (2016).
- [48] Y. Schattner, S. Lederer, S. Kivelson, and E. Berg, Ising nematic quantum critical point in a metal: A Monte Carlo study, *Phys. Rev. X* **6**, 031028 (2016).
- [49] S. Lederer, Y. Schattner, E. Berg, and S. Kivelson, Superconductivity and non-Fermi liquid behavior near a nematic quantum critical point, *Proc. Natl. Acad. Sci. U.S.A.* **114**, 4905 (2017).
- [50] T. Agatsuma and H. Yamase, Structure of the pairing gap from orbital nematic fluctuations, *Phys. Rev. B* **94**, 214505 (2016).
- [51] H. Wang, Y. Wang, and G. Torroba, Superconductivity versus quantum criticality: Effects of thermal fluctuations, *Phys. Rev. B* **97**, 054502 (2018).
- [52] D. Labat and I. Paul, Pairing instability near a lattice-induced nematic quantum critical point, *Phys. Rev. B* **96**, 195146 (2017).
- [53] P. T. Dumitrescu, M. Serbyn, R. T. Scalettar, and A. Vishwanath, Superconductivity and nematic fluctuations in a model of doped FeSe monolayers: Determinant quantum Monte Carlo study, *Phys. Rev. B* **94**, 155127 (2016).
- [54] A. Klein and A. V. Chubukov, Superconductivity near a nematic quantum critical point: Interplay between hot and lukewarm regions, *Phys. Rev. B* **98**, 220501(R) (2018).
- [55] J. A. Damia, S. Kachru, S. Raghu, and G. Torroba, Two-dimensional non-Fermi-liquid metals: A solvable large- $N$  limit, *Phys. Rev. Lett.* **123**, 096402 (2019).
- [56] A. Klein, A. V. Chubukov, Y. Schattner, and E. Berg, Normal state properties of quantum critical metals at finite temperature, *Phys. Rev. X* **10**, 031053 (2020).
- [57] J. Aguilera Damia, M. Solis, and G. Torroba, How non-Fermi liquids cure their infrared divergences, *Phys. Rev. B* **102**, 045147 (2020).
- [58] J. Aguilera Damia, M. Solis, and G. Torroba, Thermal effects in non-Fermi liquid superconductivity, *Phys. Rev. B* **103**, 155161 (2021).
- [59] G. M. Eliashberg, Interaction between electrons and lattice vibrations in a superconductor, *Sov. Phys. JETP* **11**, 696 (1960).
- [60] Y. Nambu, Quasi-particles and gauge invariance in the theory of superconductivity, *Phys. Rev.* **117**, 648 (1960).
- [61] P. K. Nag, K. Scott, V. S. de Carvalho, J. K. Byland, X. Yang, M. Walker, A. G. Greenberg, P. Klavins, E. Miranda, A. Gozar, V. Taufour, R. M. Fernandes, and E. H. da Silva Neto, Highly anisotropic superconducting gap near the nematic quantum critical point of  $\text{FeSe}_{1-x}\text{S}_x$ , *Nat. Phys.* **21**, 89 (2025).
- [62] G.-Z. Liu, Z.-K. Yang, X.-Y. Pan, and J.-R. Wang, Towards exact solutions for the superconducting  $T_c$  induced by electron-phonon interaction, *Phys. Rev. B* **103**, 094501 (2021).